

Article

Fe₃O₄ Nanoparticle-Reinforced Magnesium Nanocomposites Processed via Disintegrated Melt Deposition and Turning-Induced Deformation Techniques

Michael Johanes, Sravya Tekumalla and Manoj Gupta * 

Department of Mechanical Engineering, National University of Singapore, Singapore 117 575, Singapore; michael.johanes@u.nus.edu (M.J.); tvrlsravya@u.nus.edu (S.T.)

* Correspondence: mpegm@nus.edu.sg; Tel.: +65-6516-6358

Received: 23 October 2019; Accepted: 12 November 2019; Published: 16 November 2019



Abstract: Magnesium nanocomposites, with nano-scale ceramic reinforcements, have attracted a great deal of attention for several engineering and biomedical applications in the recent past. In this work, superparamagnetic iron oxide nanoparticles, Fe₃O₄, with their unique magnetic properties and the ability of being bio-compatible and non-toxic, are reinforced to magnesium to form Mg/(1, 2, and 3 wt %) Fe₃O₄ nanocomposites. These nanocomposites were fabricated using the conventional disintegrated melt deposition (DMD) technique followed by extrusion. Further, the materials were also processed using the novel turning-induced-deformation technique where the chips from turning process are collected, cold compacted, and hot extruded. The materials processed via the two techniques were compared in terms of microstructure and properties. Overall, the Mg/Fe₃O₄ nanocomposites, processed via both routes, exhibited a superior property profile. Further, the turning-induced deformation method showed promising results in terms of improved properties of the nanocomposites and serves as a great route for the recycling of metallic materials.

Keywords: magnesium; turning; Fe₃O₄ nanoparticles; nanocomposite; processing

1. Introduction

An upsurge in the processing and fabrication of lightweight magnesium (Mg) and the associated alloys/nanocomposites, typically for weight-sensitive applications such as in the aerospace industry, has been observed in the recent past [1–3]. A number of components in the aircraft interiors, such as passenger seats, overhead compartments, folding tables and food trolleys, and transmission casings, have the potential to use magnesium [4]. Mg nanocomposites with nanometric length scale reinforcements such as ceramic, metallic, and other carbon-based reinforcements, i.e., CNTs (carbon nanotubes) have shown promising results in improving the mechanical, physical, and ignition properties of magnesium [2,5,6]. These nanoparticles were found to have properties that alleviate certain inherent weaknesses of Mg such as limited ductility, creep resistance, and strength but, more importantly, may also be used to incorporate new, desirable, and targeted properties. So far, several techniques have been reported for the synthesis of these nanocomposites. Some of them include (i) the disintegrated melt deposition (DMD) method whereby the melt is disintegrated and deposited onto a substrate using an inert shielding gas [2]; (ii) the ultrasound assisted casting technique, to break up particle clusters in the melt [7]; (iii) the in-situ synthesis technique utilizing the self-propagating high-temperature reactions based on the thermodynamic reactions between matrix and reinforcement [8,9]. Apart from the liquid state techniques, solid state processing techniques such as powder metallurgy followed

by sintering [10] have also been popular in the production of these lightweight magnesium-based materials [11].

Conventional magnesium processing and machining, however, produces swarf/turnings, thus incurring wastage. While there have been studies on the recycling of such swarf, they were focused on re-melting for recovery of the magnesium which requires more energy than direct utilization [12]. Further studies on the recycling of magnesium turning/swarf commercially using industrial solutions are not readily available [13] while efforts on aluminum alloy machine swarf compaction methods were found, having been successfully hot-extruded into C-channels [14]. Thus, this provides a scope for a new magnesium recycling method that is more economical, via direct utilization of swarf. Such a method, named the turning-induced-deformation (TID) technique, has been recently introduced by some of the authors. This involves the consolidation of magnesium chips/turnings, followed by cold compaction and hot extrusion [15]. This technique produced extrudates with improved strength while directly utilizing machine swarf, resulting in better cost and energy efficiency owing to the fact that the chips are deformed during the turning process. The previous works dealt with the recycling of magnesium alloys. However, there has been no work on the recycling of the magnesium nanocomposites.

Hence, this work aimed to study the benefits of Fe_3O_4 nanoparticles, which have a unique combination of magnetic properties and the ability of being bio-compatible and non-toxic. Fe_3O_4 particles, being super paramagnetic in nature, have the ability to improve the electromagnetic interference (EMI) shielding effectiveness [16,17] of magnesium similar to that of iron particles, which were shown to be extremely promising [18]. These nanocomposites not only open up the possibility of applications in lightweight structural components with inherent shielding properties, but also applications in the biomedical field due to the bio-compatibility and non-toxic nature of the materials.

The focus of this work is two-fold: (i) to study and ascertain the effect of Fe_3O_4 nanoparticles on the overall properties of magnesium; (ii) to understand the properties of the magnesium nanocomposites processed using the TID technique in comparison to those processed using the conventional DMD-extrusion technique, so as to promote this technique to recycle the magnesium nanocomposites as well.

2. Materials and Methods

2.1. Materials and Processing

Magnesium turnings of 99.9% purity from Acros Organics (Morris Plains, NJ, USA) were used as the matrix material. Fe_3O_4 nanoparticles (15–30 nm) of 5.17 g/cm^3 density were used in addition to the turnings to synthesize Mg/ Fe_3O_4 nanocomposites for this study. The Mg/ Fe_3O_4 (1%, 2%, and 3%) nanocomposites were casted using the DMD technique, followed by soaking for 1 h at $400 \text{ }^\circ\text{C}$, and extrusion at $350 \text{ }^\circ\text{C}$ [19]. These materials were studied in this work to understand the effect of the presence of Fe_3O_4 nanocomposites. Further, in addition, these materials were also subjected to the turning-induced-deformation (TID) technique. In the TID technique, a conventional lathe is used to generate turnings from the cast ingots. A speed of 395 rpm, feed speed of 0.98 mm/s, and a depth of cut of 1 mm were used during the machining/turning of the ingots. The loose turnings (which are typically the industrial swarf) were collected and it was ensured that the turnings are free from contamination from foreign substances. Figure 1 below shows the cold compaction process of the turnings, from which the billets were extracted. The resulting billets were then homogenized at $400 \text{ }^\circ\text{C}$ for 1 h, followed by hot extrusion at $350 \text{ }^\circ\text{C}$ with an extrusion ratio of 20.25:1, resulting in rods of approximately 8 mm in diameter.

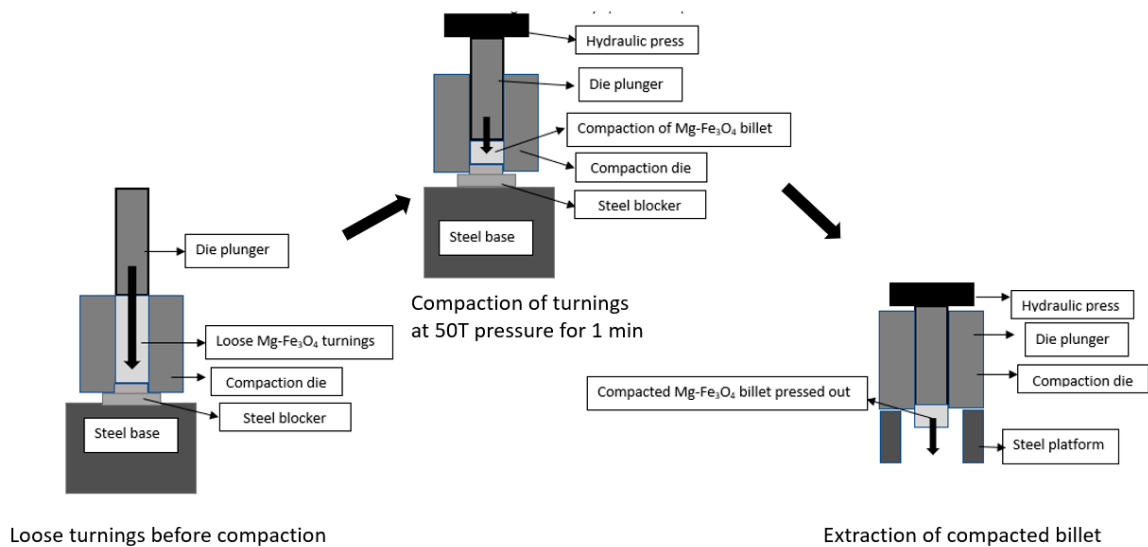


Figure 1. Schematic of the turning-induced deformation technique, showing compaction steps.

Table 1 below outlines the materials synthesized and the processing techniques and conditions used.

Table 1. Materials synthesized in this work and their processing conditions.

S. No.	Material (wt %)	Processing Technique and Conditions	Representation in This Work
1	Mg/1Fe ₃ O ₄	DMD [19] + Extrusion at 350 °C	DMD
2	Mg/2Fe ₃ O ₄	DMD [19] + Extrusion at 350 °C	DMD
3	Mg/3Fe ₃ O ₄	DMD [19] + Extrusion at 350 °C	DMD
4	Mg/1Fe ₃ O ₄	DMD [19] + TID [15] + Extrusion at 350 °C	TID
5	Mg/2Fe ₃ O ₄	DMD [19] + TID [15] + Extrusion at 350 °C	TID
6	Mg/3Fe ₃ O ₄	DMD [19] + TID [15] + Extrusion at 350 °C	TID

2.2. Physical Characterization

2.2.1. Density and Porosity

The theoretical density of the nanocomposites was calculated using the rule of mixtures. To calculate the experimental density, the gas displacement method was used to measure the density of the nanocomposite samples [20]. An AccuPyc II 1340 gas pycnometer (Norcross, GA, USA) was used to perform the measurements of the density of the nanocomposites from the two processing methods. The porosity of these samples was calculated using the assumption that the difference between the theoretical and experimental densities is due to the porosity in the materials. Average readings from 8 samples in each composition was considered as the final measurement.

2.2.2. Damping

Sample rods of ~7 mm diameter and ~55 mm length were subjected to impulse excitation by a resonance frequency damping analyzer (RFDA) acquired from IMCE, Genk, Belgium to obtain damping capacities and the elastic modulus of the nanocomposites. 10 measurements were taken for each composition to ensure consistency in the results.

2.3. Mechanical Characterization

Compression Testing

Samples of ~7 mm diameter, and a length/diameter ratio of ~1.5 were ground flat and subjected to a quasi-static compressive load in accordance with ASTM E9-09 using a MTS-810 servo-hydraulic

testing system (Eden Prairie, MN, USA) with a crosshead speed of 0.07 mm/min and the samples were compressed until failure. Five samples were tested to ensure consistency in the readings obtained and the averages of the respective readings are presented in this work.

2.4. Thermogravimetric Analysis

Samples of approximately 2 mm x 2 mm x 1 mm were subjected to heating from 30 to 750 °C with a heating rate of 10 °C/min in purified air with a flow rate of 50 mL/min using a thermo gravimetric analyzer. The resultant temperature vs. time plots were then obtained for one sample from each composition and the point with a sharp increase in temperature is determined to be the ignition temperature of the nanocomposite [3,4,21].

2.5. Microstructure Characterization

2.5.1. Grain Size Analysis

Samples from each nanocomposite were ground flat and polished using alumina suspensions, starting from 5- to 0.05-micron size. The samples were etched using a solution of 20 mL acetic acid, 1 mL HNO₃, 60 mL ethylene glycol, and 20 mL H₂O and were viewed under a Leica DM2500 optical microscope (Leica Microsystems (SEA) Pte Ltd., Singapore, Singapore) to obtain images, following which the average grain sizes of each material were ascertained with the aid of MatLab software. The average grain size obtained was later used to understand the influence of grain size on the properties of the materials.

2.5.2. Microstructure

Samples from each nanocomposite were polished and etched for observation under a scanning electron microscope. A JEOL JSM-6010PLUS/LV scanning electron microscope (SEM) (Jeol USA Inc., Peabody, MA, USA) coupled with an energy dispersive spectroscope (EDS) was utilized to investigate the key features of the nanocomposite surfaces. In addition, a chip obtained from the machining process was also observed under the scanning electron microscope to observe the features on the chips. Fractured surfaces of the samples that failed in the compression testing were also examined using SEM.

2.6. Bio-Immersion Testing

Samples from each nanocomposite (height: 1 mm, diameter: 5 mm) and processing method were ground flat and subjected to a timed corrosion test by immersing them in HBSS (Hank's balanced salt solution) at 37 °C in a temperature-controlled water bath. The samples were immersed for the durations of 1, 3, 6, 8, 15, 18, and 24 h (1 sample per duration). Once the durations elapsed, the samples were immersed in a solution consisting of 1.9 g of AgNO₃ and 20 g of CrO₃ in 100 mL of deionized water to remove the corrosion products formed on the surface, then rinsed, dried, and weighed to note down the mass loss from the corrosion-induced degradation.

3. Results

Properties of pure Mg processed using the DMD method (where included) were obtained from [21]. Pure Mg was used as a benchmark material for comparison with the Mg-Fe₃O₄ nanocomposites characterized in this study.

3.1. Microstructural Characterization

3.1.1. Grain Size Analysis

The grain characteristics of the nanocomposites processed via DMD and TID routes are given in Table 2. Figure 2 gives the representative micrographs of the samples. The Fe₃O₄ content addition lowers the mean grain diameter, i.e., the average grain size as compared to pure Mg regardless of

the method of processing, highlighting the effect of reinforcement addition to magnesium matrix. For DMD materials, increasing Fe_3O_4 content generally results in smaller grains, and the least grain size was seen in $\text{Mg}/2\text{Fe}_3\text{O}_4$. Further addition of nanoparticles led to slight grain coarsening, as seen in the mean grain diameter values of $\text{Mg}/3\text{Fe}_3\text{O}_4$. For TID materials, the grain sizes are smaller than that of DMD materials, except for $\text{Mg}/2\text{Fe}_3\text{O}_4$. Thus, the TID method is favorable, resulting in materials with finer grain sizes.

Table 2. Average grain size of $\text{Mg}/\text{Fe}_3\text{O}_4$ nanocomposites.

Nanocomposite	Processing Method	Mean Grain Diameter (μm)
Mg [21]	DMD	25 ± 4
$\text{Mg}/1\text{Fe}_3\text{O}_4$		16 ± 6
$\text{Mg}/2\text{Fe}_3\text{O}_4$		8 ± 3
$\text{Mg}/3\text{Fe}_3\text{O}_4$		10 ± 4
$\text{Mg}/1\text{Fe}_3\text{O}_4$	TID	8 ± 2
$\text{Mg}/2\text{Fe}_3\text{O}_4$		8 ± 3
$\text{Mg}/3\text{Fe}_3\text{O}_4$		9 ± 3

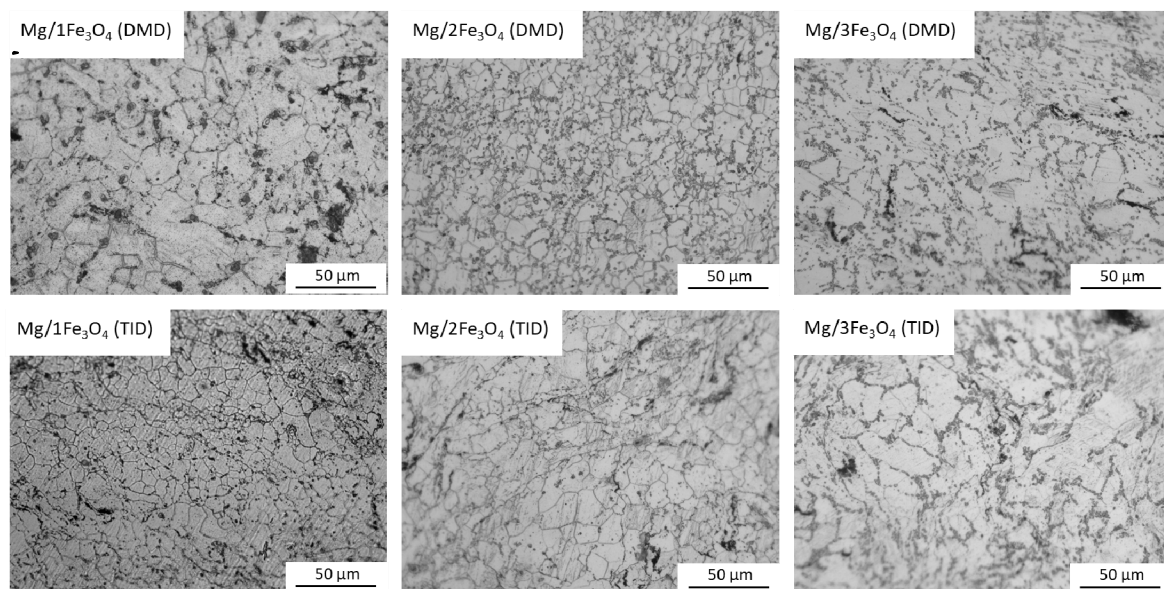


Figure 2. Optical micrographs with grains and grain boundaries of all $\text{Mg}-\text{Fe}_3\text{O}_4$ nanocomposites.

3.1.2. General Microstructure

The morphology of a typical chip produced via turning is shown in Figure 3a. The chips/turnings have two distinct regions of plastic deformation, with high and low plastic deformation regions, as shown by the presence of shear bands and as given in one of our previous works [15]. Since this deformation is induced during the turning process, we call the process of obtaining these chips and compacting them the turning-induced-deformation process.

The general microstructure of the $\text{Mg}/\text{Fe}_3\text{O}_4$ nanocomposites processed by DMD and TID techniques is given in Figure 3b,c. Fe_3O_4 particles are seen to be well dispersed in the matrix and particularly seated at the grain boundaries throughout the samples. Agglomeration of Fe_3O_4 nanoparticles was found to be a natural tendency of such nanocomposites [22], and, as such, with an increase in the Fe_3O_4 content, the nanoparticles indeed further massed in agglomerates. However, in the TID nanocomposite, a finer dispersion of Fe_3O_4 nanoparticles was seen owing to the processing method which could have randomly scattered/broken the agglomeration of the nanoparticles during the turning process. The presence of the nanoparticles at the grain boundaries confirms the Zener pinning effects of the nanoparticles in the matrix during the dynamic recrystallization process (hot extrusion) [23,24]. This led

to the reduction in the grain size due to the nanoparticles that assisted in pinning the grain boundaries, thereby increasing the grain boundary area, hindering grain growth and decreasing the grain size of the nanocomposites as compared to pure Mg. Coarsening of grain size with 3% Fe_3O_4 nanoparticles could be due to the agglomeration of the nanoparticles that reduced their pinning effects considerably.

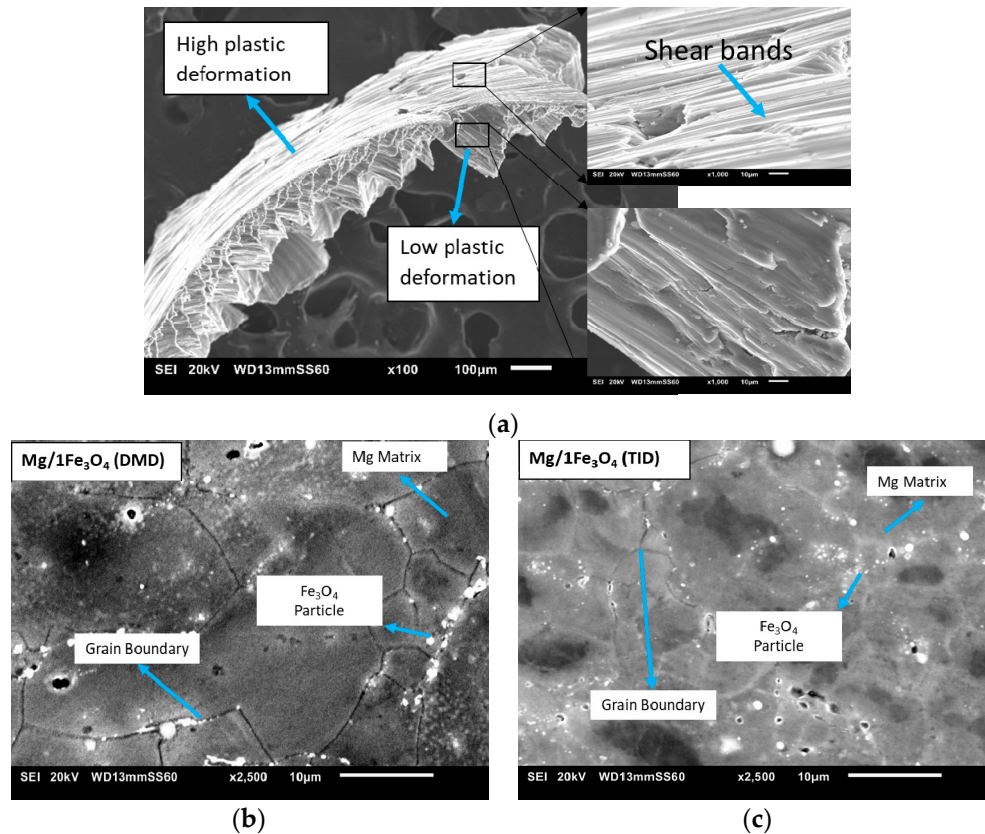


Figure 3. (a) A chip obtained via the turning of Mg/Fe₃O₄, showing low and high deformation regions; (b) the M/1Fe₃O₄ (DMD) nanocomposite; and (c) the Mg/1Fe₃O₄ (TID) with the presence of Fe₃O₄ particles seated at the grain boundaries.

3.2. Physical Properties

3.2.1. Density and Porosity

Table 3 gives the density and porosity results of the nanocomposites processed using both DMD and TID techniques. The addition of Fe₃O₄ results in the increase in density of nanocomposites due to the higher density of Fe₃O₄. Further, the porosity content also seemed to increase with increase in Fe₃O₄ content. Further, the TID samples showed marginally higher porosity levels. However, it is also observed that the experimental density of the nanocomposites remained largely the same relative to each other despite the higher theoretical density of those with higher Fe₃O₄ content, resulting in higher overall porosity levels as Fe₃O₄ content increases. The higher porosity of the TID nanocomposites is due to the presence of air gaps/voids during the compaction of turnings/chips to form a solid billet, inevitably resulting in voids and pores within the material. This is also observed in previous studies involving solid-state recycling of aluminum turnings [14], more so than the liquid phase processing, i.e., the DMD process.

Table 3. Density and porosity results of Mg/Fe₃O₄ nanocomposites obtained via both processing methods.

Nanocomposite	Processing Method	Theoretical Density (g/cm ³)	Average Experimental Density (g/cm ³)	Porosity (%)
Mg	DMD	1.74	1.73 ± 0.01	0.65
Mg/1Fe ₃ O ₄		1.77	1.76 ± 0.00	0.56
Mg/2Fe ₃ O ₄		1.81	1.78 ± 0.01	1.66
Mg/3Fe ₃ O ₄		1.84	1.79 ± 0.02	2.72
Mg/1Fe ₃ O ₄	TID	1.77	1.75 ± 0.01	1.13
Mg/2Fe ₃ O ₄		1.81	1.76 ± 0.02	2.76
Mg/3Fe ₃ O ₄		1.84	1.77 ± 0.02	3.81

3.2.2. Damping Capacity and Young's Modulus

Table 4 and Figure 4 give the damping properties of the materials. The damping capacity and attenuation coefficient increase with the progressive increase in Fe₃O₄ content in the case of both the processing methods. The highest damping capacity is observed to be in Mg/3Fe₃O₄, which is the highest damping capacity for magnesium nanocomposites recorded thus far, to the authors' best knowledge. The E-modulus is seen to decrease with increasing Fe₃O₄ content. Further, the time required to stop the vibration (Figure 4) also decreased with increasing Fe₃O₄, revealing the excellent improvement in the damping capacity of the materials with the addition of Fe₃O₄. It is to be highlighted that the TID processing of the materials showed a significant improvement in the damping capacities and no significant difference in the modulus values in comparison to the DMD samples. The highest recorded damping capacity is for the Mg/3Fe₃O₄ (TID) nanocomposite whose damping capacity was 33% higher than its DMD counterpart and 496% higher than pure Mg (DMD). This shows the TID technique as a viable route to process the materials, especially to achieve materials with excellent damping properties.

The increase in damping capacity for the TID samples were attributed to higher porosity levels (presence of air gaps in the materials) caused by compaction of turnings [25]. In addition, a prior study has shown that for processing methods resulting in high porosity, the damping capacity of the materials did indeed increase with porosity, as was done with spray-formed alloys [26] and porous magnesium [27]. The attenuation coefficient is a measure of the dampening of the curve with time, shown by the equation below ([28]):

$$A = A_0 e^{-\alpha t} + C \quad (1)$$

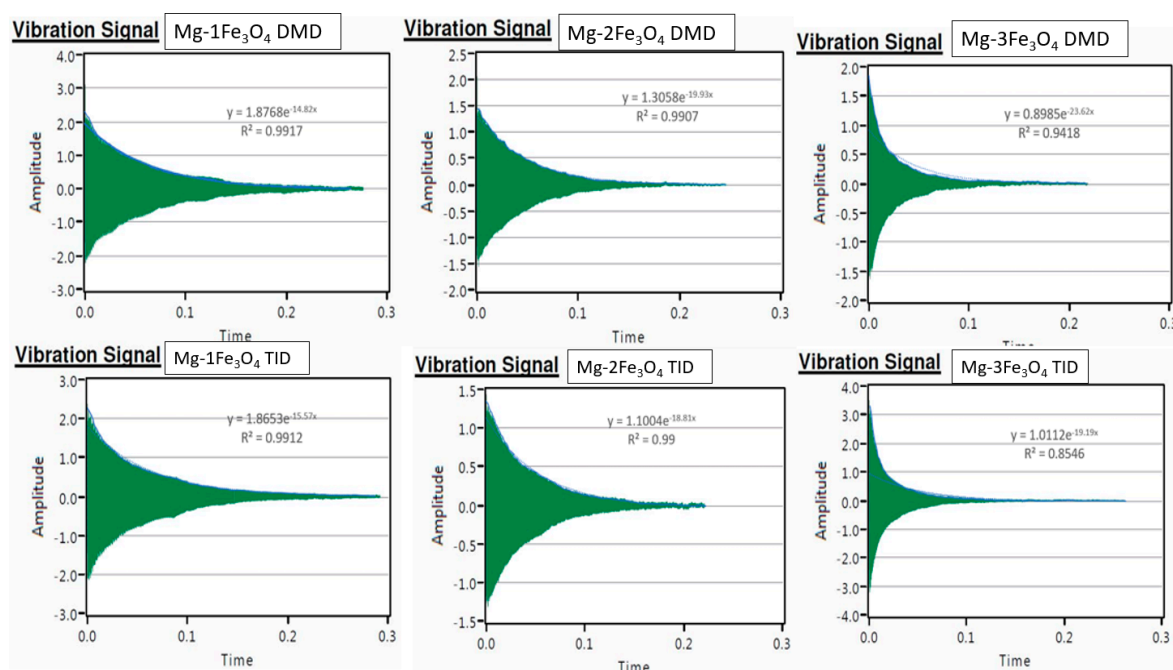
where A_0 and A are the initial and current amplitude, respectively; t is elapsed time after removal of external force; α is the apparent attenuation coefficient; and c is a fitting coefficient.

The attenuation coefficient is dependent on the resonant frequency and porosity of a material. The attenuation coefficient increased with Fe₃O₄ content, which implies that Fe₃O₄ nanoparticles can be used as dampening agents or reinforcements to magnesium and can find application in electronic, aerospace, and other engineering sectors [29].

Further, the elastic modulus of the nanocomposites, which is very critical for both engineering and biomedical applications, is seen to be marginally higher than that of Mg, i.e., ~46–49 GPa for all nanocomposites. Further, in engineering applications, stiffness is required at a minimum weight. With these materials exhibiting light weight and higher stiffness than Mg, they are well suited for engineering applications. Further, with densities and an elastic modulus fairly close to bone, the elastic mismatches between implants and bone can be eliminated with the use of these bio-compatible Mg nanocomposites [30].

Table 4. Damping property results of Mg-Fe₃O₄ nanocomposites with respect to processing methods.

Nanocomposite	Processing Method	Attenuation Coefficient	Damping Capacity	Frequency (Hz)	E-Modulus (GPa)
Mg	DMD	5.71	0.000291	6567.95	45.36
Mg/1Fe ₃ O ₄		14.82	0.000410 ± 0.000048	10528.4	49.58
Mg/2Fe ₃ O ₄		19.93	0.000673 ± 0.000179	10286.6	46.92
Mg/3Fe ₃ O ₄		23.62	0.001303 ± 0.000143	10131.5	46.05
Mg/1Fe ₃ O ₄	TID	15.57	0.000453 ± 0.000027	10409.3	48.70
Mg/2Fe ₃ O ₄		18.81	0.000690 ± 0.000022	10372.1	46.31
Mg/3Fe ₃ O ₄		19.19	0.001735 ± 0.000206	10195	46.85

**Figure 4.** Damping characteristics of Mg-Fe₃O₄ nanocomposites in terms of amplitude vs. time. Note that the scale on the Y-axis is different in each case.

3.3. Mechanical Properties (Compressive Properties)

Figure 5 shows the results of the compressive tests. The addition of Fe₃O₄ increased the yield and ultimate strengths, and the highest was observed for the Mg/2Fe₃O₄ nanocomposite, processed using the DMD method. The stress–strain plots (Figure 5), however, showed that Fe₃O₄ presence lowers ductility and energy absorbed compared to pure Mg. Progressive addition of Fe₃O₄ increased strengths but at the cost of lowering maximum deformation and forces sustained. TID processing generally exhibited higher strengths over DMD counterparts, with the ultimate compressive strength not showing significant change. Overall, Figure 5 reveals that the TID method improved yield strengths in the nanocomposites. Further, the nanocomposites processed using the TID method were found to have increased ductility and fracture strain over DMD counterparts, indicating TID to be a favorable route for materials with superior strengths and ductility.

The significant change in properties corresponds to the microstructure, i.e., presence of grains and nanoparticles. As the grain sizes were still in the micron range, the Hall–Petch relationship stands true for these materials, whereby reduction in grain sizes results in improvement of mechanical strength without sacrificing ductility [31,32]. Effective grain hardening can be achieved by reducing grain size within the microstructure [33]. Smaller grains will have a larger chance of hindering the dislocations at the grain boundary due to the increase grain boundary area [34]. Further, the TID technique helped lower the grain size further, due to the prior induced deformation in the materials.

Thus, the TID materials demonstrated improved strengths and ductilities due to the reduction in the grain size [35]. Previous studies on solid-state recycling of Al-based alloys showed resulting extrusions with high ductility [14], which aligns with the findings from this work where the materials with TID showed higher ductilities. The presence of nanoparticles also plays a significant role on the properties. With the increase in the content of nanoparticles, the strengths increased initially and dropped when the nanoparticles % was increased from 2% to 3%. This is due to the agglomeration of nanoparticles to form clusters of sub-micron to micron length scale which hampers the strength of the nanocomposite [7]. Thus, overall, the Mg/2Fe₃O₄ nanocomposite is seen to be the best in terms of the strength and ductility in both DMD and TID conditions.

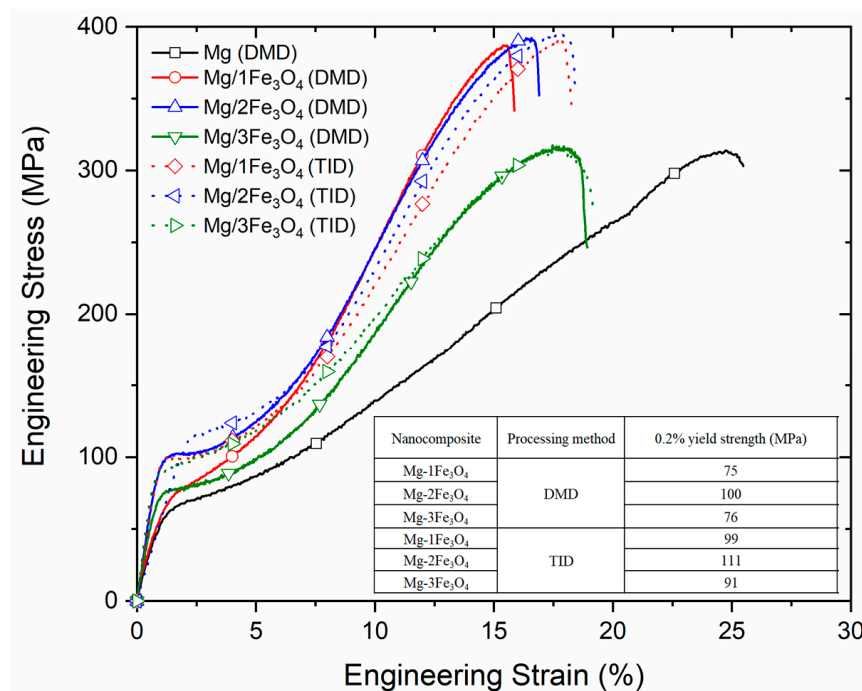


Figure 5. Stress vs strain plots of Mg–Fe₃O₄ nanocomposites under compressive loading.

Figure 6 shows the SEM images of all fracture surfaces showing the extent of plastic deformation undergone by the nanocomposites. All the nanocomposites are seen to undergo compressive failure by shear mode of deformation.

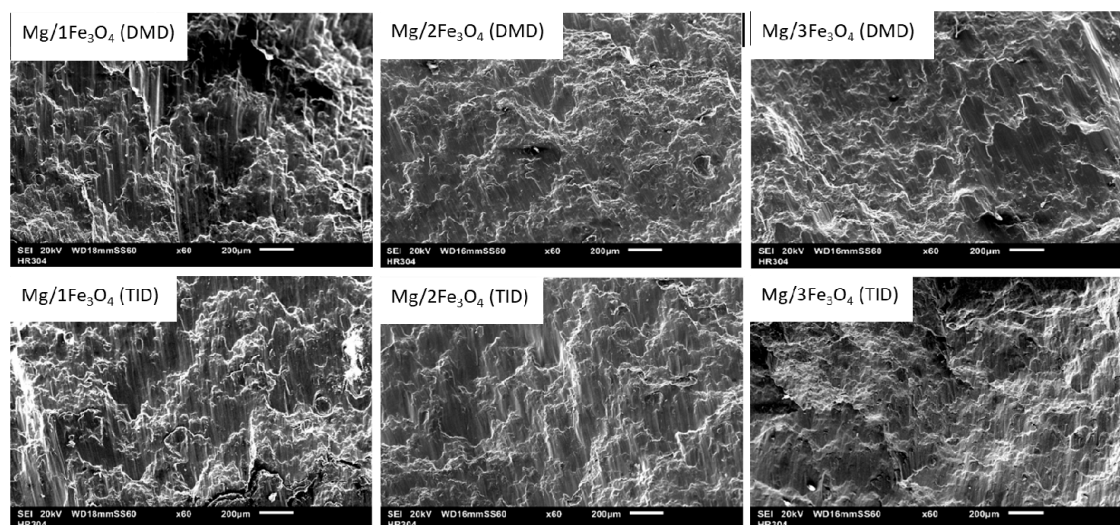


Figure 6. Compressive fractography images of all Mg–Fe₃O₄ nanocomposites.

3.4. Ignition Properties

The results of ignition temperature measurement using thermogravimetric analysis is given in Table 5. The addition of Fe_3O_4 content increases the ignition temperature and the highest ignition temperature is recorded for the Mg/3 Fe_3O_4 nanocomposite (DMD) with an ignition temperature of about 635.2 °C. There is no significant difference observed in the ignition temperatures recorded for the Mg/2 Fe_3O_4 and Mg/3 Fe_3O_4 processed via the DMD technique. A 2% addition of Fe_3O_4 can help in raising the ignition temperature by 45 °C. Although, the same trend of increase in ignition temperature with addition of Fe_3O_4 is observed in the materials processed by TID, the relative ignition temperatures values show a slight drop in ignition temperatures compared to their counterparts processed by DMD.

Table 5. Ignition test results of Mg– Fe_3O_4 nanocomposites with respect to processing methods.

Nanocomposite	Processing Method	Ignition Temperature (°C)
Mg		590
Mg/1 Fe_3O_4	DMD	630.6
Mg/2 Fe_3O_4		635.0
Mg/3 Fe_3O_4		635.2
Mg/1 Fe_3O_4		625.4
Mg/2 Fe_3O_4	TID	633.1
Mg/3 Fe_3O_4		632.2

The nanocomposites used have already displayed a marked improvement in ignition temperature when compared to pure Mg which auto-ignites at 473 °C [36] and ignites in air under a constant heating rate of 590 °C. This is likely caused by the presence of the Fe_3O_4 nanoparticles which are thermally stable and provide insulating effects to the Mg matrix surfaces by hindering heat transfer at some points, much like other oxides such as Y_2O_3 , as has been explored previously [37]. This results in elevating the ignition temperatures as Fe_3O_4 content increases. The TID nanocomposites were found to have relatively lower ignition temperatures due to the presence of higher porosity in the materials processed by the TID technique [15,38]. Better resistance to ignition is due to the formation of a relatively compact oxide layer (MgO) during oxidation that delays the further diffusion of oxygen towards Mg, prolonging the onset of ignition. With the presence of increasing porosity, the surface area exposed increases and the oxide layer is disrupted, thereby decreasing the ignition temperature. However, the TID method comes at the cost of lowering ignition temperature by only a marginal extent as compared to the DMD processing method.

3.5. Bio-Immersion Studies

The weight change in the nanocomposite samples due to immersion vs. the time of exposure of the samples (in hours) is depicted in Figure 7. The samples were immersed in HBSS solution which was maintained at normal body temperature of 37 °C. Mg/2 Fe_3O_4 (DMD) displayed the least weight change and highest resistance to bio-corrosion among all the materials. TID processed materials show increasingly higher weight change due to immersion with higher Fe_3O_4 content. The significant weight loss in the materials subjected to immersion indicates that the materials exhibit lower corrosion resistance [39]. Due to the very high rate of weight change, TID materials failed to survive immersion tests past 8 h and completely dissolved in the solution.

The TID samples dissolved and disintegrated very quickly relative to DMD samples, despite the same composition due to presence of high porosity levels in the TID samples [40]. Materials with higher porosity corrode very rapidly, as a larger area of the material surface is exposed to the corrosive environment. Further, the residual strains in the TID materials due to the prior induced deformation could also be responsible for faster degradation of the nanocomposites in the corrosive media. The behavior of the samples processed using the same technique was different because of the difference in the content of Fe_3O_4 nanoparticles, which affected the microstructure of the

nanocomposites. The Mg/Fe₃O₄ composites (DMD) however showed a similar trend of weight change compared to a significant weight change in Mg/ Fe₃O₄ (TID) composites. This was due to the porosity as well as residual strains induced during the TID process. Thus, TID materials result in quicker corrosion-induced-degradation when compared to DMD materials which is a drawback of this technique. However, porous Mg materials are desirable when used as implants due to the high biocompatibility and biodegradability of Mg [41]. Hence, further efforts need to be made in this direction to have a controlled degradability of the TID nanocomposites. Furthermore, future research in this field can involve experimentation with varying processing conditions, such as variation of turning parameters (depth of cut, feed rate, turning speed), comparison between materials produced by consolidation of turnings and consolidation of commercially-produced metal powders, as well as nanocomposite/nanoparticle variations to under the effects of the TID process.

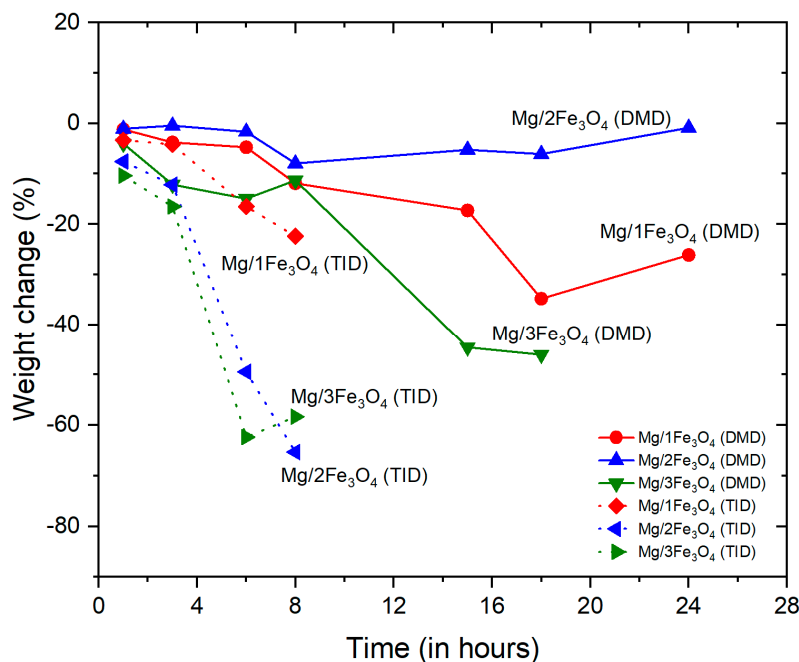


Figure 7. Wight change in the Mg–Fe₃O₄ nanocomposites with time in HBSS solution maintained at the normal body temperature of 37 °C.

4. Conclusions

This work aimed at synthesizing bio-compatible, superparamagnetic Fe₃O₄ nanoparticles to a magnesium matrix through the disintegrated melt deposition technique as well as turning-induced-deformation techniques. The following are the conclusions of this work.

1. The addition of Fe₃O₄ nanoparticles significantly enhances the damping capacity of the magnesium matrix and the highest ever damping capacity was recorded for the Mg/3Fe₃O₄ nanocomposite.
2. Further, Fe₃O₄ assists in improving the mechanical, ignition, and bio-corrosion response of magnesium and the best composition for the overall combination of properties was seen to be Mg/2Fe₃O₄ (DMD) which exhibited the lowest grain size.
3. The turning-induced-deformation (TID) method results in higher porosity as compared to the DMD method, due to which the TID nanocomposites display relatively poor ignition and bio-corrosion resistance.
4. In view of the physical and mechanical properties, the TID technique is not only economically viable and energy efficient, but also results in improvements of properties such as damping and strength.

- Hence, the proposed TID method allows for the opportunity to directly utilize otherwise discarded metal swarf without a need for remelting, greatly reducing wastage as well as increasing the proportion of metal used overall towards finished products in large-scale industrial production.

Author Contributions: Conceptualization, S.T. and M.G.; methodology, M.J.; formal analysis and investigation, M.J. and S.T.; writing—original draft preparation, M.J. and S.T.; writing—review and editing, M.J., S.T. and M.G.; project administration, S.T.; funding acquisition, M.G.

Funding: This research was funded by SINGAPORE MINISTRY OF EDUCATION, grant number WBS. R 265 000 622 112.

Acknowledgments: The authors acknowledge Juraimi Bin Madon for assistance with extrusion and Ng Hong Wei for assistance with TGA.

Conflicts of Interest: The authors declare no conflict of interest. The funders had no role in the design of the study; in the collection, analyses, or interpretation of data; in the writing of the manuscript, or in the decision to publish the results.

References

- Tekumalla, S.; Farhan, N.; Srivatsan, T.S.; Gupta, M. Nano-zno particles' effect in improving the mechanical response of mg-3al-0.4ce alloy. *Metals* **2016**, *6*, 276. [CrossRef]
- Gupta, M.; Wong, W.L.E. Magnesium-based nanocomposites: Lightweight materials of the future. *Mater. Charact.* **2015**, *105*, 30–46. [CrossRef]
- Tekumalla, S.; Gupta, M. An insight into ignition factors and mechanisms of magnesium based materials: A review. *Mater. Des.* **2017**, *113*, 84–98. [CrossRef]
- Czerwinski, F. Controlling the ignition and flammability of magnesium for aerospace applications. *Corros. Sci.* **2014**, *86*, 1–16. [CrossRef]
- Goh, C.S.; Wei, J.; Lee, L.C.; Gupta, M. Development of novel carbon nanotube reinforced magnesium nanocomposites using the powder metallurgy technique. *Nanotechnology* **2006**, *17*, 7–12. [CrossRef]
- Sankaranarayanan, S.; Jayalakshmi, S.; Gupta, M. Effect of nano-Al₂O₃ addition and heat treatment on the microstructure and mechanical properties of mg-(5.6ti+3al) composite. *Mater. Charact.* **2013**, *75*, 150–164. [CrossRef]
- Dieringa, H. Processing of magnesium-based metal matrix nanocomposites by ultrasound-assisted particle dispersion: A review. *Metals* **2018**, *8*, 431. [CrossRef]
- Tekumalla, S.; Shabadi, R.; Yang, C.; Seetharaman, S.; Gupta, M. Strengthening due to the in-situ evolution of β1' Mg-Zn rich phase in a ZnO nanoparticles introduced mg-y alloy. *Scr. Mater.* **2017**, *133*, 29–32. [CrossRef]
- Tekumalla, S.; Bibhanshu, N.; Shabadi, R.; Suwas, S.; Ha, T.M.H.; Gupta, M. Evolution of texture and asymmetry and its impact on the fatigue behaviour of an in-situ magnesium nanocomposite. *Mater. Sci. Eng. A* **2018**, *727*, 61–69. [CrossRef]
- Gupta, M.; Seetharaman, S. Using energy efficient microwaves to synthesize high performance energy saving magnesium (nano) composites. In *TMS 2015 144th Annual Meeting & Exhibition: Supplemental Proceedings*; Springer International Publishing: Cham, Germany, 2015; pp. 187–193.
- Sankaranarayanan, S.; Gupta, M. Review on mechanical properties of magnesium (nano) composites developed using energy efficient microwaves. *Powder Metall.* **2015**, *58*, 183–192. [CrossRef]
- Lapovok, R.Y.; Thomson, P.F. Production of dense rod from magnesium swarf for re-melting. *Magnes. Technol.* **2004**, *1*, 149–154.
- Nakamura, K. Introduction of grinding swarf recycling. *Ntn Technical Review No.71*, 2014. Available online: https://www.ntnglobal.com/en/products/review/pdf/NTN_TR71_en_P080.pdf(accessed on 3 January 2019).
- Chiba, R.; Yoshimura, M. Solid-state recycling of aluminium alloy swarf into c-channel by hot extrusion. *J. Manuf. Process.* **2015**, *17*, 1–8. [CrossRef]
- Tekumalla, S.; Ajjarapu, M.; Gupta, M. A novel turning-induced-deformation based technique to process magnesium alloys. *Metals* **2019**, *9*, 841. [CrossRef]
- Pandey, R.; Tekumalla, S.; Gupta, M. Enhanced (X-band) microwave shielding properties of pure magnesium by addition of diamagnetic titanium micro-particulates. *J. Alloy. Compd.* **2019**, *770*, 473–482. [CrossRef]

17. Pandey, R.; Tekumalla, S.; Gupta, M. Effect of defects on electromagnetic interference shielding effectiveness of magnesium. *J. Mater. Sci. Mater. Electron.* **2018**, *29*, 9728–9739. [[CrossRef](#)]
18. Pandey, R.; Tekumalla, S.; Gupta, M. Magnesium-iron micro-composite for enhanced shielding of electromagnetic pollution. *Compos. Part B Eng.* **2019**, *163*, 150–157. [[CrossRef](#)]
19. Jayalakshmi, S.; Singh, A.; Gupta, M. Synthesis of light metal nanocomposites: Challenges and opportunities. *Indian J. Adv. Chem. Sci. S1* **2016**, 283–288.
20. Micromeritics. Accupyc II 1340 Pycnometer. Available online: <https://www.micromeritics.com/Product-Showcase/AccuPyc-II-1340.aspx> (accessed on 3 January 2019).
21. Tekumalla, S.; Yang, C.; Seetharaman, S.; Wong, W.L.E.; Goh, C.S.; Shabadi, R.; Gupta, M. Enhancing overall static/dynamic/damping/ignition response of magnesium through the addition of lower amounts (<2%) of yttrium. *J. Alloy. Compd.* **2016**, *689*, 350–358.
22. NanoComposix. Useful Terminology. Available online: <https://nanocomposix.com/pages/useful-terminology> (accessed on 24 March 2019).
23. Tekumalla, S.; Bibhanshu, N.; Suwas, S.; Gupta, M. Superior ductility in magnesium alloy-based nanocomposites: The crucial role of texture induced by nanoparticles. *J. Mater. Sci.* **2019**, *54*, 8711–8718. [[CrossRef](#)]
24. Yang, W.; Tekumalla, S.; Gupta, M. Cumulative effect of strength enhancer—Lanthanum and ductility enhancer—Cerium on mechanical response of magnesium. *Metals* **2017**, *7*, 241. [[CrossRef](#)]
25. Atlas Foundry Company. Mechanical Properties of Gray Iron—Damping Capacity. Available online: <http://www.atlasfdry.com/grayiron-damping.htm> (accessed on 3 January 2019).
26. Li, B.; Lavernia, E.J. Damping capacity. In *Comprehensive Composite Materials*, 1st ed.; Kelly, A., Zweben, C., Eds.; Elsevier: Amsterdam, The Netherlands, 2000; Volume 3, pp. 617–653.
27. Li, Q.; Jiang, G.; Dong, J.; Hou, J.; He, G. Damping behavior and energy absorption capability of porous magnesium. *J. Alloy. Compd.* **2016**, *680*, 522–530. [[CrossRef](#)]
28. Xie, Z.-K.; Tane, M.; Hyun, S.-K.; Okuda, Y.; Nakajima, H. Vibration-damping capacity of lotus-type porous magnesium. *Mater. Sci. Eng. A* **2006**, *417*, 129–133. [[CrossRef](#)]
29. Blaney, L. Magnetite (Fe₃O₄): Properties, synthesis, and applications. *Lehigh Rev.* **2007**, *15*, 33–81.
30. Sezer, N.; Evis, Z.; Kayhan, S.M.; Tahmasebifar, A.; Koç, M. Review of magnesium-based biomaterials and their applications. *J. Magnes. Alloy.* **2018**, *6*, 23–43. [[CrossRef](#)]
31. Whang, S.H. Introduction. In *Nanostructured Metals and Alloys*; Whang, S.H., Ed.; Woodhead Publishing: Oxford, UK, 2011; pp. xxi–xxxv.
32. Chen, Y.; Tekumalla, S.; Guo, Y.B.; Shabadi, R.; Shim, V.P.W.; Gupta, M. The dynamic compressive response of a high-strength magnesium alloy and its nanocomposite. *Mater. Sci. Eng. A* **2017**, *702*, 65–72. [[CrossRef](#)]
33. Yu, H.; Xin, Y.; Wang, M.; Liu, Q. Hall-petch relationship in mg alloys: A review. *J. Mater. Sci. Technol.* **2018**, *34*, 248–256. [[CrossRef](#)]
34. Brush Wellman Inc. Grain size and material strength. In *Technical Tidbits*; Brush Wellman Inc.: Cleveland, OH, USA, 2010.
35. Gao, W.; Liu, H. A highly ductile magnesium alloy system. *IOP Conf. Ser. Mater. Sci. Eng.* **2009**, *4*, 012003. [[CrossRef](#)]
36. ToolBox, E. Fuels and Chemicals—Autoignition Temperatures. Available online: https://www.engineeringtoolbox.com/fuels-ignition-temperatures-d_171.html (accessed on 24 March 2019).
37. Tekumalla, S.; Nandigam, Y.; Bibhanshu, N.; Rajashekara, S.; Yang, C.; Suwas, S.; Gupta, M. A strong and deformable in-situ magnesium nanocomposite igniting above 1000 °C. *Sci. Rep.* **2018**, *8*, 7038. [[CrossRef](#)]
38. Tekumalla, S.; Si Chun, L.; Gupta, M. Preprocessing of powder to enhance mechanical and thermal response of bulk magnesium. *Met. Powder Rep.* **2019**, *74*, 137–140. [[CrossRef](#)]
39. Singh, I.B.; Singh, M.; Das, S. A comparative corrosion behavior of Mg, AZ31 and AZ91 alloys in 3.5% NaCl solution. *J. Magnes. Alloy.* **2015**, *3*, 142–148. [[CrossRef](#)]
40. Březina, M.; Minda, J.; Doležal, P.; Krystýnová, M.; Fintová, S.; Zapletal, J.; Wasserbauer, J.; Ptáček, P. Characterization of powder metallurgy processed pure magnesium materials for biomedical applications. *Metals* **2017**, *7*, 461. [[CrossRef](#)]

41. Tan, L.; Yu, X.; Wan, P.; Yang, K. Biodegradable materials for bone repairs: A review. *J. Mater. Sci. Technol.* **2013**, *29*, 503–513. [[CrossRef](#)]



© 2019 by the authors. Licensee MDPI, Basel, Switzerland. This article is an open access article distributed under the terms and conditions of the Creative Commons Attribution (CC BY) license (<http://creativecommons.org/licenses/by/4.0/>).